Thermal Scanning at the Cellular Level by an Optically Trapped Upconverting Fluorescent Particle

*Paloma Rodríguez-Sevilla, Yuhai Zhang, Patricia Haro-González, Francisco Sanz-Rodríguez, Francisco Jaque, José García Solé, Xiaogang Liu, and Daniel Jaque**

Photothermal treatment of cancer cells consists in a controlled heating above their physiological temperature (37 °C) by means of an external light source. Therapeutic effects of such heating arise from the activation of different biological, physical, and chemical phenomena that could result in permanent or temporal modifications at the cellular level.[1] The alterations induced in the treated cells strongly depend on the amount of heating, ranging from transient to irreversible damage when temperature is increased from 41 up to 60 °C.[2] Despite the existence of different cell damage types, there is still a big lack of knowledge concerning the exact cellular mechanisms responsible of them. Such knowledge requires the design and performance of photothermal experiments at the single-cell level. The simultaneous developing of nanotechnology and bioimaging techniques has made such experiments possible. First results evidenced that a proper interpretation of single-cell photothermal treatments needs an accurate monitoring of both intracellular and extracellular temperatures.[3] While intracellular temperature is necessary to explain the damage induced in the cell under treatment, the exact knowledge of the thermal gradient created in its surroundings is fundamental to explain the damage appearing in neighboring cells.[4] The magnitude and extension of thermal gradients in the surrounding of cells and other heating objects in aqueous media have been estimated and postulated in the past, but neither has been experimentally measured.[5]

Thermal sensing at the cellular level should be achieved with minimum perturbation, i.e., in absence of physical contact between cells and sensing units.[4,6,7] Among the different approaches proposed for contactless cellular sensing, the use of luminescent thermometry (LT) has been found to be especially interesting.[8,9] LT is based on the use of luminescent probes (luminescent thermometers, LThs) which optical properties show a remarkable temperature dependence.[8,10–12] In most cases, thermal sensing at cellular level has been achieved after massive incorporation of LThs into the cells. Based on this approach, several groups have managed to get high resolution thermal images of living cells and individual living organisms during photothermal treatments.[6,12,13] Nevertheless, such a massive incorporation could lead to the appearance of undesirable cytotoxic effects.[14] An alternative approach consists in the incorporation into the cellular environment of a single LTh that could be remotely controlled.[15,16] Optical trapping (OT) is a versatile and reliable noncontact tool for 3D manipulation of colloidal micro/nano sized objects.[17–19] OT is based on the forces exerted by a tightly focused laser beam on micro/nanoparticles due to momentum exchange or to the field induced changes in their polarizability. OT of colloidal LThs is, in principle, possible with the additional advantage of simultaneous excitation of their luminescence if the wavelength of the trapping beam is tuned to any absorption band of the LTh. Under this approach, thermal reading at the laser trap position (through particle luminescence) and 3D localization of LTh, become possible.[19,20] Despite the great potential of this approach and its apparent technical simplicity, it still remains an unexplored possibility.

In this work we have demonstrated that thermal scanning at the cellular level is possible by a simple single-beam–single-particle approach. The novelty of this approach is that it involves simultaneous OT and luminescence analysis of a single LTh. This possibility has been demonstrated by using colloidal $NaYF_4$:Er^{3+},Yb^{3+} particles as sensing units. The choice of such particular crystal particles is motivated by their outstanding ratiometric thermal sensitivity (>10^{-2} °C^{-1}).[10] The potential of OT-assisted contactless thermal sensing for in vitro studies has been demonstrated by measuring the thermal gradients created in the surroundings of a single cancer cell subjected to a plasmonic mediated photothermal therapy.

Figure S1a in the Supporting Information includes the scanning electron microscopy (SEM) images and size histograms of the different $NaYF_4$:Er^{3+},Yb^{3+} particles used in this work. Up to four different hexagonal $NaYF_4$:Er^{3+},Yb^{3+} particles have been investigated, with dimensions (thickness, diameter) of (0.4, 0.8 μm), (0.5, 1.5 μm), (0.7, 2 μm), and (1.6, 3 μm), respectively. All the samples showed a high structural quality (see Figure S1b in the Supporting Information) as well good colloidal stability in distilled water. **Figure 1**a shows the experimental setup used for OT of a single $NaYF_4$:Er^{3+},Yb^{3+} particle (see Figure 1b). A diluted aqueous solution of $NaYF_4$:Er^{3+},Yb^{3+} particles was

P. Rodríguez-Sevilla, Dr. P. Haro-González, Dr. F. Sanz-Rodríguez, Prof. F. Jaque, Prof. J. G. Sole, Dr. D. Jaque
Fluorescence Imaging Group
Departamento de Física de Materiales
Facultad de Ciencias
Universidad Autonoma de Madrid
Madrid 28049, Spain
E-mail: daniel.jaque@uam.es

P. Rodríguez-Sevilla, Dr. P. Haro-González, D. Jaque
Instituto Nicolás Cabrera
Universidad Autónoma de Madrid
Madrid 28049, Spain

Y. Zhang, Prof. X. Liu
Department of Chemistry
National University of Singapore
3 Science Drive 3, Singapore 117543, Singapore

Dr. F. Sanz-Rodríguez, Dr. D. Jaque
Instituto Ramón y Cajal de Investigaciones Sanitarias
Hospital Ramón y Cajal
Madrid 28034, Spain

DOI: 10.1002/adma.201505020

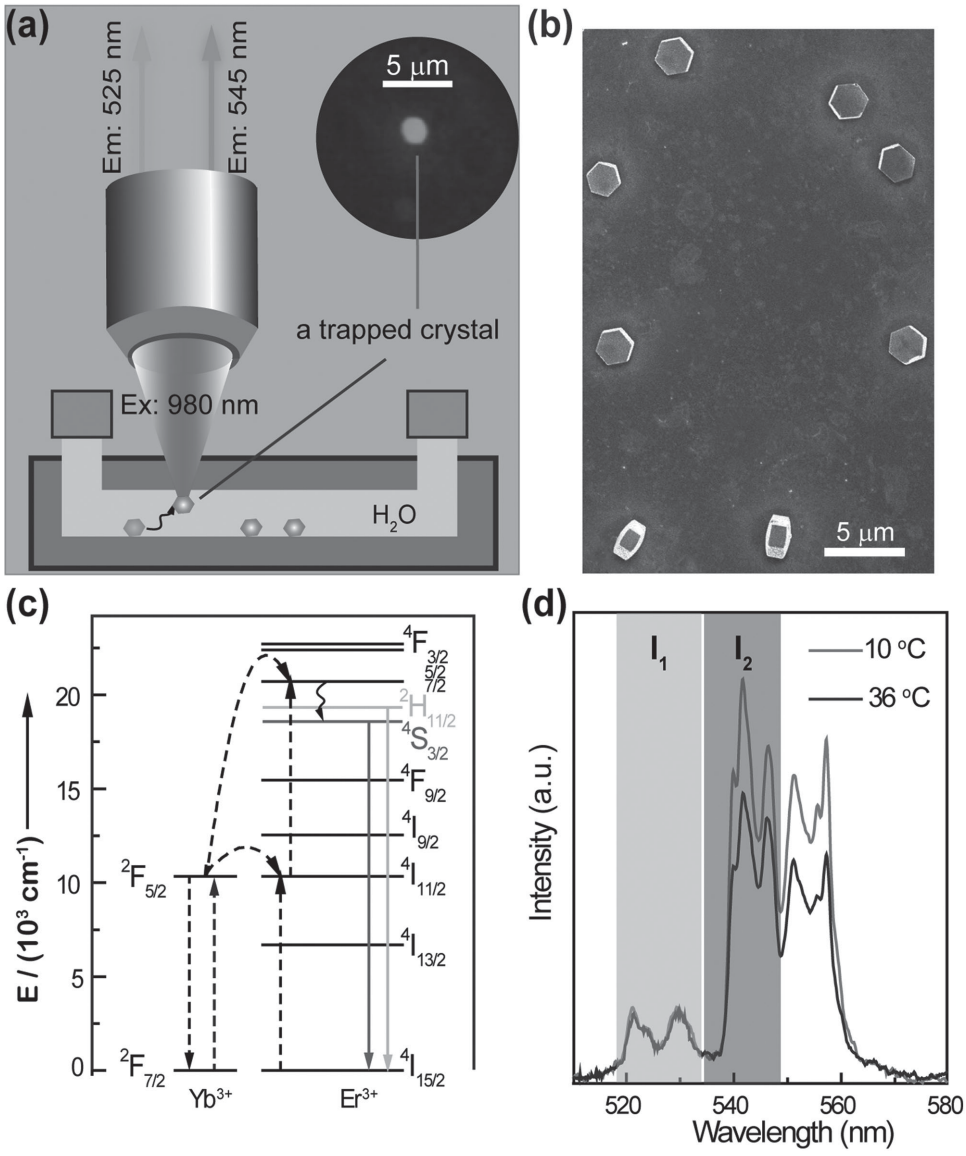

Figure 1. a) Schematic representation of the experimental setup used in this work for thermal sensing by an optically trapped $NaYF_4:Er^{3+},Yb^{3+}$ particle (5/0.5 mol%). b) A typical scanning electron microscopy image of $NaYF_4:Er^{3+},Yb^{3+}$ particle, showing a clear hexagonal morphology. c) Simplified energy level diagram showing the temperature sensitive energy levels, $^2H_{11/2}$ and $^4S_{3/2}$, and the corresponding energy transition processes. d) Emission spectra obtained from a single optically trapped $NaYF_4:Er^{3+},Yb^{3+}$ particles at two different temperatures. The intensity ratio I_1/I_2 is highly temperature-sensitive.

introduced in a microchannel, into which a 980 nm laser beam was tightly focused by a single microscope objective. When a $NaYF_4:Er^{3+},Yb^{3+}$ particle is optically trapped, a strong green emission is generated from the trap, as it can be observed in Figure 1a as well as in the representative video included in Video S1 in the Supporting Information. This green emission, generated by Er^{3+} ions, results from a process known as energy-transfer assisted upconversion (see the schematic energy level diagram of Figure 1c) that has been widely used for biosensing and bioimaging.[21–23] A typical upconversion spectrum in the 500–570 nm spectral range generated by an optically trapped $NaYF_4:Er^{3+},Yb^{3+}$ particle is included in Figure 1d. As can be observed in Figure 1d, Er^{3+} ions show two intense bands centered at 525 and 550 nm that correspond to the $^2H_{11/2}\rightarrow{}^4I_{15/2}$ and $^4S_{3/2}\rightarrow{}^4I_{15/2}$ transitions, respectively (see Figure 1c).[10] As these emission bands are generated from two thermally coupled excited states, the ratio between their emitted intensities is strongly temperature dependent allowing for accurate thermal sensing.[21,23] Figure 1d shows the luminescence spectra generated by an optically trapped $NaYF_4:Er^{3+},Yb^{3+}$ particle (3 μm in diameter) as obtained when the aqueous dispersion temperature was set to 10 and 36 °C. As can be observed, a rise in temperature causes an increment in the intensity ratio, $R = I_1/I_2$ ratio, between the 540 and 525 nm bands. This is due to the temperature-induced increase (decrease) of the population of the $^2H_{11/2}$ ($^4S_{3/2}$) excited state.[21] Figure S2 in the Supporting Information shows the temperature dependence of the intensity ratio R as obtained from an optically trapped $NaYF_4:Er^{3+},Yb^{3+}$

(data obtained varying the medium temperature). The observed linear relation between R and temperature evidences that the local temperature can be accurately measured from the analysis of the luminescence generated by the optically trapped particle. Thermal sensitivity of LThs, S, is typically defined as $S = (dR/dT)(R)^{-1}$. Linear fit of the data included in Figure S2 in the Supporting Information leads to a thermal sensitivity close to $1.6 \times 10^{-2} \pm 0.1 \times 10^{-2}$ °C^{-1} at 25 °C. This thermal sensitivity is found to be in good agreements with those previously reported for other Er^{3+},Yb^{3+} systems.[21] At this point it should be noted that the spectral distribution of the upconversion spectrum generated by individual $NaYF_4$:Er^{3+},Yb^{3+} particles has been found to slight vary from particle to particle as it is shown in Section S4 in the Supporting Information.

The possibility of 3D manipulation and scanning of a single $NaYF_4$:Er^{3+},Yb^{3+} particle by OT in a cellular medium would depend on the magnitude of the optical forces exerted on it that should overcome drag forces created by fluid viscosity. The magnitude of OT forces acting on the different $NaYF_4$:Er^{3+},Yb^{3+} particles was measured by the hydrodynamic drag method, as explained in detail in Section S3 in the Supporting Information.[18,24] A representative force versus power plot is included in **Figure 2**a, from which the trapping constant (K_{trap}, OT force divided by laser power) can be calculated. K_{trap} was found to be strongly dependent on both the Numerical Aperture (NA) of the microscope objective and the $NaYF_4$:Er^{3+},Yb^{3+} particle size as it was expected.[16] This fact is evidenced in Figure 2b,c. Figure 2b shows the dependence of K_{trap} on the $NaYF_4$:Er^{3+},Yb^{3+} particle size as obtained for a microscope objective of NA = 0.8 that produces a laser spot diameter close to 1.4 µm. These were found to be the optimum trapping conditions for the 2 µm diameter $NaYF_4$:Er^{3+},Yb^{3+} particles. This fact suggests that the optical force is maximized when the $NaYF_4$:Er^{3+},Yb^{3+} particle diameter slightly exceeds the laser spot diameter. This suggestion has been corroborated in Figure 2c, in which we have systematically investigated the OT force acting on 3 µm sized $NaYF_4$:Er^{3+},Yb^{3+} particles as a function of the NA of the focusing objective. OT force is maximum when the NA is set to 0.55, which leads to a laser spot diameter of 2.2 µm (slightly smaller than particle size). From Figure 2c it is clear that an adequate choice of focusing optics could lead to trapping constants as large as 60 fN mW^{-1}, allowing for their stable scanning in the surroundings of cells by using moderate laser trapping powers. In this sense we have to note that, as discussed in Section S5 in the Supporting Information, upconversion from single particles can be detected by using 980 nm laser powers as low as 1 mW (0.3×10^5 W cm^{-2} power density). Nevertheless, the laser power used during the radial thermal scans was set to be 13 mW (3.6×10^5 W cm^{-2} power density) as it ensures thermal resolutions of 1 °C while keeping the thermal loading induced by trapping radiation close to 1 °C (see Section S5 in the Supporting Information).[25]

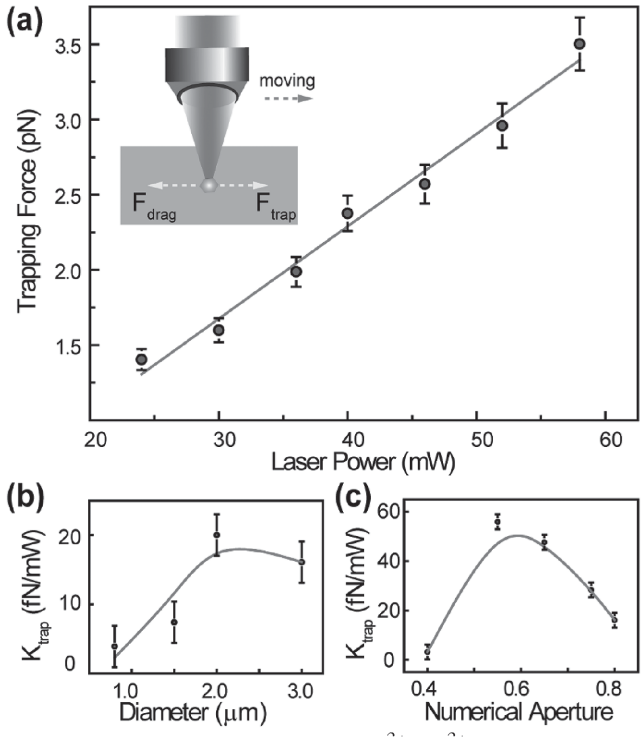

Figure 2. a) Optical trapping force on a $NaYF_4$:Er^{3+},Yb^{3+} particles as a function of the 980 nm laser power. Numerical aperture of the focusing objective was 0.55. The inset shows a diagram indicating how the optical force is measured in this work. b) Optical trapping constant (K_{trap}) as a function of the diameter of the particle. Data were obtained using a NA = 0.8 focusing objective. Dots correspond to the experimental data and the solid line is a guide for the eyes. c) Optical trapping constant (K_{trap}) as obtained for a 3 µm in diameter $NaYF_4$:Er^{3+},Yb^{3+} particles as a function of the numerical aperture of the focusing objective. The dots are the experimental data and the solid line is a guide for the eyes.

Once simultaneous OT and thermal sensing from a single $NaYF_4$:Er^{3+},Yb^{3+} particle had been demonstrated, we combined them to elucidate the magnitude and spatial extension of the thermal gradient created in the surroundings of a cancer cell subjected to a plasmonic based photothermal treatment. For such a purpose, we designed the experimental approach schematically represented in **Figure 3**a that implies the scanning of an optically trapped $NaYF_4$:Er^{3+},Yb^{3+} particle in the surroundings of a HeLa cell. Cells were previously incubated with 15 × 45 nm gold nanorods (GNRs). These GNRs have a surface plasmon resonance wavelength peak close to 800 nm (see Figure S3, Supporting Information) and a heating efficiency close to unity.[10,26] Efficient intracellular incorporation of GNRs was verified by multiphoton fluorescence microscopy (see **Figure 4**a and Figure S3, Supporting Information). The incorporation of GNRs allowed for intracellular heating by using an 800 nm laser beam that was focused into the cell by means of a single microscope objective. For thermal measurements in the surroundings of the treated cell, $NaYF_4$:Er^{3+},Yb^{3+} particles were added to the culture medium. A 980 nm laser beam was used for OT and scanning of a single $NaYF_4$:Er^{3+},Yb^{3+} particle. OT and particle scanning in the surroundings of a cell should overcome several difficulties that are discussed in detail in Section S6 in the Supporting Information. The extension and magnitude of thermal gradients in the surroundings of individual cells was investigated by performing different "horizontal" thermal scans at different particle-to-substrate distances. As explained the Supporting information, the performance of horizontal scans minimizes the possible influence of particle-to-substrate interaction in the output thermal

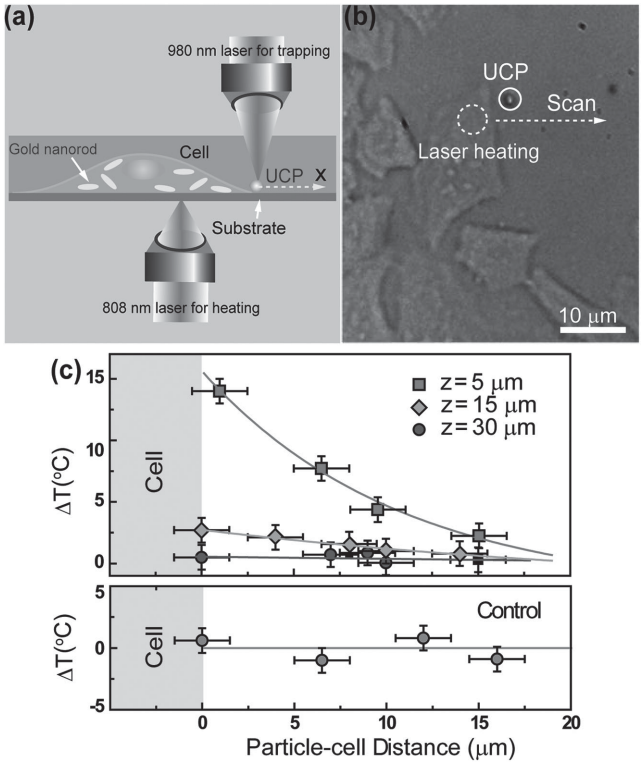

Figure 3. a) Schematic representation of the experimental setup used for thermal scanning in the surroundings of a HeLa cell subjected to a plasmonic mediated photothermal treatment. The thermal scan direction is indicated with an arrow. b) The optical-transmission image of the HeLa cancer cells after incubation with GNRs. The dashed circle indicates the position of the (heating) 800 nm laser spot. The presence of the $NaYF_4$:Er^{3+},Yb^{3+} particle used for thermal measurements is also indicated by a dashed circle. c) Upper part: Temperature decay measured from cell surface for three heights (distances from substrate). The symbols are the experimental data, and the lines are a guide for the eyes. Lower part: Control thermal scan performed in absence of the 800 nm heating laser.

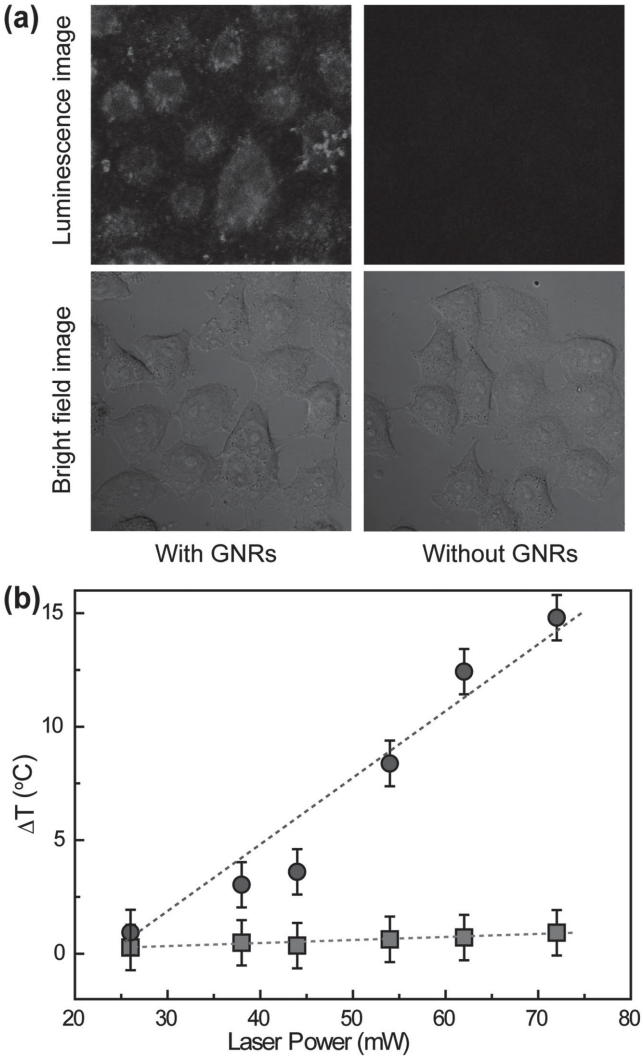

Figure 4. a). Luminescence (upper part) and optical (lower part) images of the used HeLa cells incubated with (left) and without (right) GNRs. A clear difference in the luminescence denotes the presence of GNRs inside the cells. b). Maximum temperature increment induced in the surrounding of a cell incubated with (circles) and without (squares) as a function of the laser power of the 800 nm laser heating. The dashed lines are linear fits.

reading. Figure 3b shows an $NaYF_4$:Er^{3+},Yb^{3+} particle (3 μm in diameter, indicated by a dashed circle) that has been optically manipulated in the proximity of a HeLa cancer cell incubated with GNRs. The location of the 800 nm heating laser spot inside the HeLa cancer cell has been indicated by a dashed circle. The dashed arrow indicates the horizontal scan pathway. The temperature increment (in respect to medium temperature, T_{med} = 27 °C) sensed by the $NaYF_4$:Er^{3+},Yb^{3+} particle at different horizontal (x) distances from the cell as obtained at different z heights are included in Figure 3c, where symbols correspond to the experimental data and the lines are a guide for the eyes (details about temperature and spatial uncertainties can be found in Section S5 in the Supporting Information). Figure 3c also includes (bottom graph) the "control" thermal scan obtained when the 800 nm laser beam was switched off, revealing the 800 nm laser radiation as the unique heating source. Figure 4b shows the magnitude of the extracellular heating as a function of the 800 nm laser power as obtained for control and GNRs incubated cells. It is found that, for cells containing GNRs, the maximum extracellular temperature increases linearly with laser power as it was expected. In absence of internalized GNRs (control experiment), no heating was observed. This reveals GNRs as the unique light-to-heat conversion particles.

From the thermal scans included in Figure 3c, it is clear that plasmonic mediated heating is not restricted to the intracellular volume. On the contrary, thermal gradients extend to distances larger than 10 μm. The existence of such thermal gradients makes real single-cell photothermal treatment not feasible since not only the treated cell but also all cells in its surroundings will be heated. The extension of the thermal gradient (λ_T) is here defined as the distance at which temperature has been reduced down to 0.5 times the maximum temperature (achieved at the beginning of the scan). From data included in Figure 3c we have estimated $\lambda_T \approx 6$ μm that is close to the effective radius of the 800 nm laser focal volume. According to the discussion included in Section S7 in the

Supporting Information, this suggests that the treated cell is acting as a point heating source. Note that the analysis of the horizontal scans obtained at different heights also evidences the existence of a vertical thermal gradient with an extension of few micrometers (when the z coordinate is increased from 5 up to 15 µm the magnitude of extracellular heating is reduced by almost 80%).

As is explained in Section S7 in the Supporting Information, the extension of thermal gradients is expected to be strongly dependent on the geometry of the heating source. For instance, the extension of thermal gradients created by a cylindrical heating source in a microfluidic chamber is expected to be of the order of the chamber height. In order to double check the validity of our approach for the determination of thermal gradients we designed an additional control experiment that is schematically represented in Figure S9a in the Supporting Information. In this case, the thermal gradient was created by focusing a 1480 nm laser beam (partially absorbed by water, see Figure S10 in the Supporting Information) into a 100 µm height microchannel. The spatial extension of the thermal pattern created by water absorption has been measured by scanning an optically trapped $NaYF_4:Er^{3+},Yb^{3+}$ particle in an orthogonal direction to the 1480 nm laser beam path. The experimentally measured temperature profile is shown in Figure S9a in the Supporting Information. The highest temperature (that is proportional to the 1480 nm laser power as shown in Figure S9b in the Supporting Information) was obtained at the focus of the 1480 nm laser beam. From the temperature profile included in Figure S9 in the Supporting Information, a thermal gradient extension of 100 µm was obtained, being this comparable to the chamber height. This well agrees with theoretical predictions for heating source with cylindrical symmetry, as is explained in detail in Section S7 in the Supporting Information. Such excellent agreement confirms the reliability of our approach for accurate determination of thermal gradients at the microscale.

3. Conclusion

In summary, this work demonstrates how thermal sensing in the surroundings of a single cancer cell with a micrometer-scale spatial resolution and a sub-degree thermal accuracy is possible by remote (contactless) scanning of a single optically driven/excited luminescent thermometer. This has been demonstrated by scanning an optically trapped $NaYF_4:Er^{3+},Yb^{3+}$ upconverting particle. Partial absorption of the 980 nm trapping laser beam allowed for simultaneous 3D manipulation and fluorescence ratiometric thermal sensing by using a simple experimental design. This novel approach has been used to elucidate the magnitude and spatial extension of the thermal gradient appearing in the surroundings of a plasmonic mediated photothermally treated cancer cell. Thermal gradient has been found to extend over 10 µm affecting surrounding cells and avoiding single-cell treatment.

Results included in this work constitute the first step toward the achievement of minimally invasive, contactless, high-sensitivity 3D thermal imaging of microsized systems. The results here reported constitute the proof of concept and a wide working field is now open for the optimization of the thermal sensing particle and 3D optical trapping systems.

4. Experimental Section

$NaYF_4:Er^{3+},Yb^{3+}$ Particle Synthesis: The $NaYF_4:Er^{3+},Yb^{3+}$ particles were synthesized by the hydrothermal method. More details about the synthesis process can be found in the Supporting Information.

Optical Trapping: $NaYF_4:Er^{3+},Yb^{3+}$ particles were optically trapped in a homemade single-beam optical-tweezers setup. Laser radiation coming from a 980 nm single-mode fiber-coupled laser diode was used for both trapping and exciting the $NaYF_4:Er^{3+},Yb^{3+}$ particle. The hydrodynamic drag method was used to calculate the optical forces exerted over the different particles. Details about force calculation procedure and the optical system used for optical trapping experiments can be found in the Supporting Information.

Thermal Sensing: Luminescence spectra of optically trapped $NaYF_4:Er^{3+},Yb^{3+}$ particles was spectrally analyzed by a high sensitivity Si CCD camera (Synapse, Horiba) attached to a monochromator (iH320, Horiba) all it optically coupled to the single-beam opticaltweezers setup. Calibration curves were acquired by varying the temperature of the aqueous solution contained the optically trapped $NaYF_4:Er^{3+},Yb^{3+}$ particle while performing simultaneous spectrum acquisition and analysis. Thermal resolution had been estimated from the signal/noise ratio of upconverted spectra to be ±1°C. More detail can be found in the Supporting Information.

Cell Preparation: Single-cell plasmonic mediated photothermal treatments were performed on HeLa cancer cells after incubation with gold nanorods with surface plasmon resonance at 808 nm. An 800 nm fiber coupled laser diode was focused into a HeLa cell promoting plasmonic mediated heating. The heating laser power was set to 15 mW. Further details about the cell preparation procedure can be found in the Supporting Information.

Supporting Information

Supporting Information is available from the Wiley Online Library or from the author.

Acknowledgements

This work was supported by the Spanish Ministerio de Educación y Ciencia (MAT2013–47395-C4–1-R) and by Banco Santander for "Proyectos de Cooperación Interuniversitaria" (2015/ASIA/06). P.H.G thanks the Spanish Ministerio de Economía y Competitividad (MINECO) for the Juan de la Cierva program. P.R.S thanks the Spanish Ministerio de Economía y Competitividad (MINECO) for the "Promoción del talento y su Empleabilidad en I+D+i" statal program.

Received: October 12, 2015
Revised: November 12, 2015
Published online: January 28, 2016

[1] a) J. Van der Zee, *Ann. Oncol.* **2002**, *13*, 1173; b) P. Wust, B. Hildebrandt, G. Sreenivasa, B. Rau, J. Gellermann, H. Riess, R. Felix, P. M. Schlag, *Lancet Oncol.* **2002**, *3*, 487.

[2] a) A. Chicheł, J. Skowronek, M. Kubaszewska, M. Kanikowski, *Rep. Pract. Oncol. Radiother.* **2007**, *12*, 267; b) M. Johannsen, U. Gneveckow, L. Eckelt, A. Feussner, N. Waldofner, R. Scholz, S. Deger, P. Wust, S. A. Loening, A. Jordan, *Int. J. Hyperthermia* **2005**, *21*, 637; c) J. Mendecki, E. Friedenthal, C. Botstein, R. Paglione, F. Sterzer, *Physics* **1980**, *6*, 1583; d) E. Day, P. A. Thompson, L. Zhang, N. A. Lewinski, N. Ahmed, *J. Neuro-Oncol.* **2011**, *104*, 55; e) W. Zhang, Z. Guo, D. Huang, Z. Liu, X. Guo, H. Zhong, *Biomaterials* **2011**, *32*, 8555; f) C. J. Diederich,

Int. J. Hyperthermia **2005**, *21*, 745; g) R. W. Habash, R. Bansal, D. Krewski, H. T. Alhafid, *Crit. Rev. Biomed. Eng.* **2007**, *35*, 37; h) S. V. Torti, F. Byrne, O. Whelan, N. Levi, B. Ucer, M. Schmid, F. M. Torti, S. Akman, J. Liu, P. M. Ajayan, O. Nalamasu, D. L. Carroll, *Int. J. Nanomed.* **2007**, *2*, 707; i) B. J. Wood, Z. Neeman, A. Kam, *Tumor Ablation*, Springer, New York **2005**, p. 285.

[3] H. Y. Nam, S. M. Kwon, H. Chung, S.-Y. Lee, S.-H. Kwon, H. Jeon, Y. Kim, J. H. Park, J. Kim, S. Her, Y.-K. Oh, I. C. Kwon, K. Kim, S. Y. Jeong, *J. Controlled Release* **2009**, *135*, 259.

[4] L. M. Maestro, P. Haro-Gonzalez, M. C. Iglesias-de la Cruz, F. Sanz-Rodriguez, A. Juarranz, J. G. Sole, D. Jaque, *Nanomedicine* **2013**, *8*, 379.

[5] a) N. Manuchehrabadi, L. Zhu, *Int. J. Hyperthermia* **2014**, *30*, 349; b) R. Singh, K. Das, S. C. Mishra, *J. Therm. Biol.* **2014**, *44*, 55; c) A. AlAmiri, K. Khanafer, K. Vafai, *Num. Heat Transfer Part A—Appl.* **2014**, *66*, 1; d) G. Baffou, R. Quidant, C. Girard, *Phys.Rev. B* **2010**, *82*, 165424.

[6] a) F. Wang, D. Banerjee, Y. Liu, X. Chen, X. Liu, *Analyst* **2010**, *135*, 1839; b) D. K. Chatterjee, M. K. Gnanasammandhan, Y. Zhang, *Small* **2010**, *6*, 2781.

[7] D. Jaque, B. del Rosal, E. Martin Rodriguez, L. Martinez Maestro, P. Haro-Gonzalez, J. Garcia Sole, *Nanomedicine* **2014**, *9*, 1047.

[8] a) D. Jaque, F. Vetrone, *Nanoscale* **2012**, *4*, 4301; b) C. D. S. Brites, P. P. Lima, N. J. O. Silva, A. Millan, V. S. Amaral, F. Palacio, L. D. Carlos, *New J.Chem.* **2011**, *35*, 1177.

[9] C. D. S. Brites, P. P. Lima, N. J. O. Silva, A. Millan, V. S. Amaral, F. Palacio, L. D. Carlos, *Nanoscale* **2012**, *4*, 4799.

[10] F. Vetrone, R. Naccache, A. Zamarron, A. J. de la Fuente, F. Sanz-Rodriguez, L. M. Maestro, E. M. Rodriguez, D. Jaque, J. G. Sole, J. A. Capobianco, *ACS Nano* **2010**, *4*, 3254.

[11] a) M. A. Bennet, P. R. Richardson, J. Arlt, A. McCarthy, G. S. Buller, A. C. Jones, *Lab Chip* **2011**, *11*, 3821; b) U. Rocha, C. Jacinto, W. F. Silva, I. Guedes, A. Benayas, L. M. Maestro, M. A. Elias, E. Bovero, F. van Veggel, J. A. G. Sole, D. Jaque, *ACS Nano* **2013**, *7*, 1188; c) C. Gota, K. Okabe, T. Funatsu, Y. Harada, S. Uchiyama, *J. Am. Chem. Soc.* **2009**, *131*, 2766; d) L. Shang, F. Stockmar, N. Azadfar, G. U. Nienhaus, *Angew. Chem. Int. Ed.* **2013**, *52*, 11154.

[12] a) J. S. Donner, S. A. Thompson, M. P. Kreuzer, G. Baffou, R. Quidant, *Nano Lett.* **2012**, *12*, 2107; b) A. P. Sudarsan, V. M. Ugaz, *Proc. Natl. Acad. Sci. USA* **2006**, *103*, 7228.

[13] a) G. Baffou, H. Rigneault, D. Marguet, L. Jullien, *Nat. Methods* **2014**, *11*, 899; b) J.-M. Yang, H. Yang, L. Lin, *ACS Nano* **2011**, *5*, 5067; c) J. S. Donner, S. A. Thompson, C. Alonso-Ortega, J. Morales, L. G. Rico, S. I. C. O. Santos, R. Quidant, *ACS Nano* **2013**, *7*, 8666.

[14] K. Okabe, N. Inada, C. Gota, Y. Harada, T. Funatsu, S. Uchiyama, *Nat. Commun.* **2012**, *3*, 705.

[15] a) L. Aigouy, L. Lalouat, M. Mortier, P. Löw, C. Bergaud, *Rev. Scientific Instrum.* **2011**, *82*, 036106; b) E. Hemmer, N. Venkatachalam, H. Hyodo, A. Hattori, Y. Ebina, H. Kishimoto, K. Soga, *Nanoscale* **2013**, *5*, 11339; c) L. Aigouy, A. Cazé, P. Gredin, M. Mortier, R. Carminati, *Phys. Rev. Lett.* **2014**, *113*, 076101.

[16] L. Aigouy, G. Tessier, M. Mortier, B. Charlot, *Appl. Phys. Lett.* **2005**, *87*, 1.

[17] a) M. Dienerowitz, M. Mazilu, K. Dholakia, *J. Nanophotonics* **2008**, *2*, 021875; b) H. Zhang, K. K. Liu, *J. R. Soc. Interface* **2008**, *5*, 671; c) A. Ashkin, *Proc. Natl. Acad. Sci. USA* **1997**, *94*, 4853; d) A. Ashkin, J. M. Dziedzic, T. Yamane, *Nature* **1987**, *330*, 769.

[18] W. H. Wright, G. J. Sonek, M. W. Berns, *Appl. Opt.* **1994**, *33*, 1735.

[19] P. M. Bendix, L. Jauffred, K. Norregaard, L. B. Oddershede, *IEEE J. Quantum Electron.* **2014**, 20.

[20] a) P. Haro-Gonzalez, W. T. Ramsay, L. M. Maestro, B. del Rosal, K. Santacruz-Gomez, M. D. Iglesias-de la Cruz, F. Sanz-Rodriguez, J. Y. Chooi, P. R. Sevilla, M. Bettinelli, D. Choudhury, A. K. Kar, J. G. Sole, D. Jaque, L. Paterson, *Small* **2013**, *9*, 2162; b) F. M. Mor, A. Sienkiewicz, L. Forró, S. Jeney, *ACS Photonics* **2014**, *1*, 1251.

[21] P. Haro-Gonzalez, B. del Rosal, L. M. Maestro, E. Martin Rodriguez, R. Naccache, J. A. Capobianco, K. Dholakia, J. G. Sole, D. Jaque, *Nanoscale* **2013**, *5*, 12192.

[22] a) T. V. Gavrilović, D. J. Jovanović, V. Lojpur, M. D. Dramićanin, *Sci. Rep.* **2014**, *4*, 4209; b) F. Auzel, *J. Lumin.* **1990**, *45*, 341; c) N. Phuong-Diem, S. J. Son, J. Min, *J. Nanosci. Nanotechnol.* **2014**, *14*, 157; d) S. Zeng, Z. Yi, W. Lu, C. Qian, H. Wang, L. Rao, T. Zeng, H. Liu, H. Liu, B. Fei, J. Hao, *Adv. Funct. Mater.* **2014**, *24*, 4196; e) Y. I. Park, H. M. Kim, J. H. Kim, K. C. Moon, B. Yoo, K. T. Lee, N. Lee, Y. Choi, W. Park, D. Ling, *Adv. Mater.* **2012**, *24*, 5755; f) S. H. Nam, Y. M. Bae, Y. I. Park, J. H. Kim, H. M. Kim, J. S. Choi, K. T. Lee, T. Hyeon, Y. D. Suh, *Angew. Chem.* **2011**, *123*, 6217.

[23] F. Auzel, *Chem. Rev.* **2004**, *104*, 139.

[24] K. Dholakia, P. Reece, M. Gu, *Chem. Soc. Rev.* **2008**, *37*, 42.

[25] P. Haro-González, W. T. Ramsay, L. M. Maestro, B. del Rosal, K. Santacruz-Gomez, M. del Carmen Iglesias-de la Cruz, F. Sanz-Rodríguez, J. Y. Chooi, P. R. Sevilla, M. Bettinelli, D. Choudhury, A. K. Kar, J. G. Solé, D. Jaque, L. Paterson, *Small* **2013**, *9*, 2162.

[26] a) D. Jaque, L. Martinez Maestro, B. del Rosal, P. Haro-Gonzalez, A. Benayas, J. L. Plaza, E. Martin Rodriguez, J. Garcia Sole, *Nanoscale* **2014**, *6*, 9494; b) L. M. Maestro, P. Haro-Gonzalez, A. Sanchez-Iglesias, L. M. Liz-Marzan, J. Garcia Sole, D. Jaque, *Langmuir* **2014**, *30*, 1650.